Al_2O_3-H_2O nanofluids for cooling PEM fuel cells: a critical assessment

Aimen Zeiny [a, b, *]; Maher A.R. Al-Baghdadi [b]; Ward F. Arear [b]; Mohammed S. Ismail [c]

[a] Nanotechnology and Advanced Materials Research Unit, Faculty of Engineering, University of Kufa, Najaf, Iraq

[b] Department of Mechanical Engineering, Faculty of Engineering, University of Kufa, Najaf, Iraq; mahirar.albaghdadi@uokufa.edu.iq; wardarear25@gmail.com

[c] Energy Institute, University of Sheffield, Sheffield S3 7RD, UK; m.s.ismail@sheffield.ac.uk

[*] Correspondence: aimen.zeiny@uokufa.edu.iq

Abstract Polymer electrolyte membrane (PEM) fuel cells are promising eco-friendly and sustainable power generation technology. Thermal management of these cells is one of the main challenges facing their commercialization. Alumina nanofluids, in addition to others, have been proposed to overcome excess heat generated within the PEM fuel cell stacks. However, most the previous studies investigated the hydrothermal performance of the nanofluids as a function of Reynolds number (Re). It is evident that all parameters must be kept constants except one to examine its effect on the performance. To this end, choosing Re as a parameter (independent variable) is problematic as it is a function not only of nanofluid's velocity, but also its density and viscosity. In this study, a well-validated CFD model has been built to simulate the hydrothermal performance of alumina nanofluids of different volumetric concentrations (0%, 0.05%, 0.1% and 0.2%) as functions of Re ($170 < Re < 530$) , flow rate (20 ml/min $\leq V_f \leq$ 50 ml/min), and pumping power (0.025 mW < Pp < 0.3 mW). This study shows a maximum reduction of 7.9% in the thermal effectiveness and a maximum increase of 6% in the pumping power when using the nanofluids instead of water. This deterioration in the hydrothermal performance is due to the reduction in the effective specific heat capacity and increase in viscosity of the nanofluids. Also, it is concluded that it is incorrect to use Re as an independent variable in analysing the hydrothermal performance of nanofluids because of the dependency of Re on some of the thermophysical properties of the nanofluids, which are functions of the concentration. Adopting such analysing procedure leads to false conclusions.

Keywords: fuel cell; cooling management; hydrothermal performance; nanofluid

Nomenclature

Symbols	
A_{cs}	Cross-section area of the channel [m^2]
C_p	Specific heat capacity [J/kg.K]
D_h	Hydraulic diameter [m]
h	Heat transfer coefficient [$W/m^2.K$]
k	Thermal conductivity [W/(m.K)]
k_s	Thermal conductivity of the aluminium plate [W/(m.K)]
m	Mass [kg]
Nu	Nusselt number
p	Pressure [Pa]
Pc	Pumping power required to reduce the IUT by 1ºC [W/ºC]
Pp	Pumping power [W]
Re	Reynolds number
T	Temperature [K]
u	Velocity [m/s]
V	Flow rate [ml/min]
W	Cross-section's side length of the cooling channel [m]
Abs	Absorbance [cm^{-1}]
Greek symbols	
Δp	Pressure drop [Pa]
ΔT	Temperature change [K]
ϵ	Emissivity
ε	Effectiveness of the coolant, which represent the rate change of the IUT with the pumping power [ºC/W]
μ	Dynamic viscosity [Pa.s]
ρ	Density [m^3/kg]
σ	Stefan-Boltzmann constant, $1.38x10^{-23}$ [J/K]
$\emptyset$	Volumetric concentration of the nanoparticles
λ	Wave length [nm]
Subscriptions	
amb	Ambient
bf	Base-fluid
f	Fluid
nf	Nanofluid
mp	Metal piece
Abbreviations	
IUT	Index of uniform temperature
PEM	Polymer electrolyte membrane

1. Introduction

Hydrogen PEM fuel cells are a competitive clean and sustainable energy conversion technology. This technology is one of the promising solutions to global warming and environmental pollution issues. Applying this technology to transportation and power generation sectors can rehabilitate our sick planet as the by-products of the electrochemical reaction inside the hydrogen PEM fuel cell are, in addition to electricity, water vapour and heat [1,2]. However, the efficiency and the lifespan of these fuel cells are dependent on parameters such as the operating temperature and pressure, relative humidity, material properties and design [3]. Among these parameters, the temperature and its homogeneity inside the PEM fuel cells are critical. This criticality is because the electrochemical reaction, water formation, dehydration, mass transportation and material degradation (membrane electrode assembly, MEA) within a PEM fuel cell are sensitive to the temperature and its distribution [4,5]. Thus, the index of uniform temperature (IUT) was suggested by Chen F.C.et al. [6] – as an analysis method to reach the optimal convective heat transfer by a cooling plate – to be adopted later in many studies [7–11]. This index shows the difference between the local temperature and the mean temperature of the entire cooling plate (the lower the IUT is, the lower difference between the maximum and the mean temperatures, which is an important measure to prevent the membrane dry-out) [6].

For high power generation PEM fuel cell stacks, thermal management is crucial [12,13] since about 58% of the fuel energy is converted to heat [14]. Liquid cooling is preferable to air cooling in high power generation PEM fuel cells due to the high cooling capacity of liquids compared to air. Water and water-ethylene glycol mixture are the most common coolants used in the thermal management of PEM fuel cells. However, these common coolants are suffering from relatively low thermal conductivity compared to solids; therefore, suspending nanoparticles into these coolants has been proposed recently to increase their thermal conductivity, to enhance the heat transfer rate within the fuel cells, and to improve the efficiency of the thermal management process [4].

Since the early proposal of Choi [15] to use nanofluids as alternative heat transfer media, many studies have been conducted to identify parameters that affecting their effective thermal conductivity. Shi Y. et al. [16] used a molecular dynamic simulation to study the shape effects of iron nanoparticles added to water on the thermal performance of the resulting nanofluid. They concluded that spherical iron nanoparticles could improve the thermal conductivity significantly to achieve a value of 1.35 W/m.K. While Younes H et al. [17] reviewed critically the key parameters that can enhance the thermal conductivity of nanofluids. They found that the material, shape, and size of the nanoparticles, in addition to the surfactant and solvent types, which are added to the base fluid, have direct effects on the final thermal conductivity. The effect of suspending non-spherical (i.e., tube, fiber, rod, ellipsoid, platelate, brick, and diamond) nanoparticles in the base fluids was reviewed by Li X. et al. [18]. After collecting and analysing the experimental data on heat transfer enhancement of

nanofluids, they concluded that, although abnormal high thermal conductivities were reported when using high aspect ratio nanoparticles (i.e., carbon nanotubes/nanofibers), improved, negligible, and even deteriorated hydrothermal performance were achieved depending on which figure of merit was employed in the analysis. Like the thermal conductivity, the other thermophysical properties of a fluid (e.g., density, specific heat capacity and viscosity) can be affected by dispersing nanoparticles in it. Hence, it is crucial to examine those effects on the heat transfer since the convective heat transfer depends on all these thermophysical properties.

Many researchers have studied the convective heat transfer using nanofluids as heat transfer media [19,20], and efforts have been done to identify the main mechanisms behind the enhancement of heat transfer. Brownian diffusion and thermophoresis were concluded to be the dominant slip mechanisms that can produce relative motion between the nanoparticles and the base fluid, which could intensify turbulence in nanofluids [21]. These findings have encouraged researchers to utilise nanofluids in many applications, and thermal management of PEM fuel cell stacks is one of these applications [22]. Thus, three main research areas have been emerged: i) research focuses on the synthesis and/or preparation of new nanofluids and their characterisation, e.g., measuring the thermal and electrical conductivity, viscosity, specific heat capacity, etc. [23–31]. This area aims to synthesis a cheap, eco-friendly and nontoxic nanofluids with desirable properties such as high thermal conductivity and heat capacity, low viscosity and electrical conductivity, and high density; ii) research focuses on evaluation the employment of nanofluids on the whole thermal management system of PEM fuel cells or its components (i.e., fuel cell stacks, pumps, radiators and fans) [32–34]. This area aims to optimise the thermal management system design so that the size and cost of its components can be reduced. iii) area focuses on the effect of using nanofluids on controlling the fuel cell stack's temperature and its homogeneity. As mentioned earlier, the temperature and its homogeneity within the fuel cells are critical parameters as they affect their performance and longevity, efforts have been made to investigate this research area, as reviewed below.

Zakaria I. et al. [35] investigated experimentally the effect of suspending Al_2O_3 nanoparticles (0.1% and 0.5% volume concentration) in water (H_2O)-ethylene glycol (EG) mixture (50% volume concentration) on the convective heat transfer and pumping power. The results showed that each heat transfer coefficient (h), Nusselt number (Nu), and pumping power (Pp), as functions of Re, increase as the volumetric concentration of the nanoparticles (Ø) increases. The highest percentage increases in h and Pp were 15.2% and 58% when Ø and Re were 0.5% and 120 respectively. The researchers interpreted this enhancement in the convective heat transfer coefficient as mainly due to the increase in the effective thermal conductivity. However, they numerically found that the percentage increases in h and Pp were 7.3% and 37% respectively (Ø=0.5% and Re 150). In another study, Zakaia I. et al. [36] experimentally analysed the employment of aqueous silica nanofluids in cooling a PEM fuel cell. Silica nanoparticles were dispersed in distilled water to prepare different nanofluid concentrations (0.1%, 0.3%, and 0.5%) to be pumped at different inlet Reynold's

numbers ($750 \leq Re \leq 900$) to a cooling plate subjected to a constant heat flux. They found that, like the reduction of the average plate temperature, both *h* and Δp could be increased by increasing the nanofluid's concentration. Therefore, they included the advantage ratio (AR), which is the ratio between the heat transfer enhancement and the increase in the pumping power. They finally concluded that aqueous silica nanofluids could be potential alternatives to water in cooling PEM fuel cells. Usri et al. [37] also investigated the convective heat transfer utilizing Al_2O_3-H_2O-EG (Ø = 0.2%, 0.4% and 0.6%). They presented Nu and *h* as functions of Re and found that both Nu and *h* increase as Ø increases. However, they did not calculate the pumping cost for their experiments. On the other hand, Guzei et al. [38] conducted laminar convective heat transfer experiments and studied the impact of Ø on pressure drop (Δp), *h* and Nu. They employed different concentrations ($0.25\% \leq Ø \leq 6\%$) of different nanoparticles (Al_2O_3, TiO_2, ZrO, and diamond) at different sizes (from 5 nm to 150 nm). They presented h, Nu, and Δp as functions of Re, where $100 < Re < 1500$. Again, the main finding was; h, Nu, and Δp increase as Ø increases. Similarly, the same finding, i.e., the effect of Ø on Nu and Δp, was achieved by Khetib Y. et al. [39], by conducting a numerical study to evaluate the hydrothermal performance of a DWCNTs-TiO_2/water nanofluid flowing in a pipe employing different turbulators for a large range of Reynolds number ($7000 \leq Re \leq 28000$). The heat transfer performance of alumina and silica aqueous nanofluids used in a PEM fuel cell was investigated by Zarizi M. et al. [40]. They presented the wall temperature change of a cooling channel, *h* and Nu as functions to Re, which varied between 300 and 700. All these parameters, at a specific Re, were higher for the nanofluids than the distilled water. Also, hybrid nanofluids by dispersing alumina nanoparticles and silica nanoparticles at different ratios once in water [41] and second in a water: bio glycol mixture [42] were evaluated as coolants for a PEM fuel cell. Again, the h, Nu, and Δp were presented as functions to Re. Both studies suggested the hybrid nanofluids, at a certain mixing ratio, as alternative coolants having higher heat transfer performances than their counterparts and the base fluid. Different hybrid nanofluids composed of titania and silica nanoparticles mixed at different portions with water: ethylene glycol mixture were tested experimentally by Zakaria I. et al. [43]. They found the hybrid nanofluid can reduce the thermal resistance (R_{th}) and can increase the heat transfer coefficient (*h*), in addition to electrical power loss, compared to the base fluid.

In all reviewed papers above, the thermal performance of the different nanofluids was evaluated by one analysis strategy, i.e., examining h, Nu, R_{th}, AR and/or Δp as functions to Re; however, one can criticize this analysis strategy because Re is not only a function of the nanofluid's velocity but is a function of its viscosity too. Therefore, since the effective viscosity of the nanofluids is sensitive to the concentration of the nanoparticles, one can expect that the velocity of the nanofluids must increase to keep the same Re, compared to the base fluids. Consequently, *h*, and Nu increase since the convective heat transfer is sensitive to the flow rate at low Re. Furthermore, unlike the IUT, *h* and Nu do not indicate the uniformity of the temperature distribution within a PEM fuel cell, which is critical to its performance and lifespan.

Thus, another strategy is required to analyse the hydrothermal performance of the nanofluids.

Pumping power (Pp) is an important parameter in most engineering applications, and it is a function of the pressure drop and flow rate of heat transfer media. Therefore, studying the thermal performance of the nanofluids as a function of pumping power is more appropriate. However, investigating the thermal performance, presented by the IUT, as a function to Pp instead of Re is still lacking, and this research aims to cover this shortcoming. Therefore, the IUT has been examined as functions to the volume flow rate (V_f), Re, and Pp in this study for comparison purpose. Moreover, two parameters have been derived and introduced in order to check the feasibility of using nanofluids in PEM fuel cell applications. First of which is the effectiveness (ε) of the coolant which represents the rate change of the IUT with the Pp (°C/mW), and second of which is the pumping cost (Pc) which represents the rate change of the pumping power with the IUT (mW/°C).

2. Methodology

A comprehensive CFD model was built and utilised to investigate the hydrothermal performance of a typical PEM fuel cell cooling plate. Also, nanofluids were prepared and characterised to use their thermophysical properties in the CFD model. In addition, an experimental setup was set for validation purposes. The detailed methods are presented in the following subsections.

2.1. Nanofluid preparation and characterisation

Al_2O_3-H_2O was chosen since most of the published papers stated that using this type of nanofluids could enhance the thermal performance of the cooling plates. For preparation, a hydrophilic Al_2O_3 nanopowder (purchased from US Research Nanomaterials, Inc. Hoston, USA with ɣ-type, 99$^+$% purity, 20 nm average diameter) was added to deionised water and stirred for 15 min and then sonicated according to the procedure mentioned by R.R.R. Marin et.al [44]. Four volumetric concentrations were prepared: 0 %, 0.05%, 0.1% and 0.2%. The size and shape distributions of the Al_2O_3 nanoparticles suspended in water were examined using a transmitted electron microscope, TEM (Zeiss, model EM10C). A small droplet of well sonicated diluted alumina nanofluid was put on the TEM grid by using a 20 µl pipette. The grid with the nanofluid sample was left for 1.5 hr to ensure all water was evaporated, leaving a thin layer of Al_2O_3 nanoparticles. With self-closing tweezers, the grid was put on the sample holder, and the latter was inserted inside the TEM microscope. The result is shown in Figure 1. Different shapes (i.e., spherical, oval and cylindrical) can be seen. This result is comparable with the result obtained by Y. Zhai et. al. [45].

Two techniques, namely visual characterisation and UV-Vis spectrometry, were adopted in this study to check the stability of the prepared nanofluids. Figure 2 shows photographic pictures for the nanofluids after one day, two days, seven days, and 30

days respectively. The observations are in accordance with those reported in [46]. The dependency of a nanofluid's absorbance on the size and shape of the nanoparticles makes the UV-Vis spectrophotometry one of the common techniques, which can indicate the status of the aggregation/agglomeration of the nanoparticles [47]. By using a T90+ UV/Vis spectrophotometer from PG Instrument Limited, UK, the spectrometry results for the alumina nanofluids are shown in Figure 3. Figure 3 (a) shows a linear relationship between the absorbance and the concentration of the nanofluid, which is in an excellent agreement with the Lambert-Beer's law. While Figure 3 (b) shows the spectral absorbance of the nanofluid as a function of its concentration and age. Clearly, a storing time of 7 days caused small change in the absorbance values. Also, it was found that subjecting the samples to five minutes of sonication can keep the absolute change in the absorbance within 1%. Therefore, this measure was applied before each experiment.

For nanofluid characterization purpose, a Hoppler falling-ball viscometer (DIN 53015, 0.6 mPa.s ≤ η ≤ 250000mPa.s, -20ºC≤ T ≤ 120 ºC) was used to measure the viscosity. Each test was repeated three times to calculate the mean and standard deviation values. A KD2 Pro thermal properties analyser from Decagon Devices, Inc. was employed in measuring the thermal conductivity. On the other hand, the density of the nanofluids was calculated from the measured mass and volume. Namely, the volume of the nanofluids was measured by using a standard volumetric measuring flask, while the mass was measured by using an electronic analytical balance (Wiggen Hauser Company, 0.0001 g sensitivity). For the specific heat capacity calculation, the principle of energy balance was adopted. A piece of metal of known mass and specific heat capacity was heated up using a water bath at specified temperature and kept for a while to ensure the thermocouple sensor reads a constant temperature. This meant both the water and the metal piece were in thermal equilibrium. After that, the metal piece was taken out and put in a well-insulated container, which contained known mass of the nanofluid. The thermal energy moved from the hot metal piece to the relatively cold nanofluid. When the thermocouple sensor reached a constant temperature reading (in other words the thermal equilibrium between the metal piece and the nanofluid was reached), this temperature reading was used to calculate the specific heat capacity of the nanofluid according to the following energy balance equation:

$$c_p m\,\Delta \mathrm{T}\big]_{\mathrm{nf}} = c_p m\,\Delta \mathrm{T}\big]_{\mathrm{mp}} \qquad (1)$$

where $c_p, m, \Delta \mathrm{T}$ are the specific heat capacity, mass, and temperature change respectively for both the nanofluids and the metal piece.

Each test was repeated three times in the characterisation phase and the average and the standard deviation values were calculated. The results are shown in Figure 4, which demonstrates the ratio of the nanofluid's property (P_{nf}) to the base-fluid property (P_{bf}) as a function to nanoparticle concentration (Ø). Clearly, all the thermophysical properties (i.e., ρ, *k,* and μ) are directly proportional to Ø except C_p which is inversely

proportional to Ø. The relationships between $\frac{P_{\mathrm{nf}}}{P_{\mathrm{bf}}}$ and Ø were curve-fitted to linear (the coefficients of determination (R^2) were found to be greater than 0.999). Also, it is obvious that the measured ρ and C_p had the lowest standard deviation values while the measured μ and k had the highest values; this is attributed to the use of hand stopwatch in viscosity measurements and accompanied convection in thermal conductivity measurements. However, those values of the standard deviation were fairly sufficient to obtain precise CFD simulations as will be seen in section 3.

2.2. Experimental set-up

Figure 5 shows the experimental setup, which is used for validation purposes. A home-made cooling plate having a typical serpentine channel (2mm x 2mm) was manufactured by machining a plate of aluminium (100 mm x 100 mm x 5 mm) using a CNC fraser machine. A 10-mm thick clear plastic sheet was used as a cover for the aluminium plate to see if there are any bubbles within the flow. A 1 mm-thick Teflon sheet was used as a gasket between the aluminium cooling plate and the clear cover to prevent any leakage. Three well-calibrated K-type thermocouples were used in this setup to measure each of the lab temperature, the inlet temperature and the outlet temperature of the working fluid. Also, a well-calibrated flowmeter (ZYIA, model LZM-4T, 6-60ml/min) was used to control the flow rate through the cooling plate. A constant heat transfer was fed to the cooling plate by fixing a flat cell heater to its bottom base. The cell heater was covered by a layer of glass wool to minimize the losses to the environment. A data logger (Applent, model AT 4532) was employed to display and save the temperatures.

2.3. Cooling plate computational model

2.3.1. Governing equations

The coolant's flow through the serpentine channel is assumed to be incompressible, single-phase, and laminar. The flow field is obtained by solving the steady-state Navier-Stokes equations [48].

The continuity equation is given by:

$$\nabla.(\rho.u) = 0 \quad (2)$$

The momentum equation is expressed as:

$$(u.\nabla)\rho.u = -\nabla \mathrm{p} + \mu.\nabla^2 u \quad (3)$$

The energy equation is given by:

$$u.\nabla \mathrm{T} = \frac{k}{\rho\, C_p}\nabla^2 \mathrm{T} \quad (4)$$

where $\rho, u, \mathrm{p}, \mu, \mathrm{T}, k\ and\ C_p$ are the density [m^3/kg], velocity [m/s], pressure [Pa], dynamic viscosity [Pa.s], temperature [K], thermal conductivity [W/(m K)] and specific heat capacity [J/(kg K)] of the coolant respectively.

While the energy equation for the solid region is given by [48]:

$$k_s \nabla^2 \mathrm{T} = 0 \quad (5)$$

where k_s is the thermal conductivity of the aluminium plate.

Any external surface convects and radiates heat to the ambient according to the following equation;

$$-\mathbf{n}.(-k\nabla \mathrm{T}) = h(\mathrm{T_{amb}} - \mathrm{T}) + \epsilon\left(\mathrm{T_{amb}}^4 - \mathrm{T}^4\right) \quad (6)$$

where n is the unit vector normal to the surface, h is the convection coefficient [W/m^2.K], $\mathrm{T_{amb}}$ is the ambient temperature [K], ϵ is the emissivity and σ is Stefan-Boltzmann constant, which is 1.38x10^{-23} [J/K].

2.3.2. Computational procedure and boundary conditions

The computational domain represents a cooling plate as shown in *Figure 6*. A serpentine flow channel of 2mm side length square cross-section is generated on the upper surface. **Table 1** shows the Dimensions and material properties of the cooling plate. A finite element method was adopted in discretizing and solving the governing equations by using a commercial CFD software, COMSOL Multiphysics®. A test was conducted to inspect the solution's independence of the CFD model of the grid size. The test checked the dependencies of the temperature and pressure differences of the working fluid between the outlet and inlet of the cooling channel. The relative errors, $\left[\left(\Delta \mathrm{T}_{\mathrm{mesh}_{(n+1)}} - \Delta \mathrm{T}_{\mathrm{mesh}_{(n)}}\right)/\Delta \mathrm{T}_{\mathrm{mesh}_{(n+1)}}\right]$, and $\left[\left(\Delta \mathrm{p}_{\mathrm{mesh}_{(n+1)}} - \Delta \mathrm{p}_{\mathrm{mesh}_{(n)}}\right)/\Delta \mathrm{p}_{\mathrm{mesh}_{(n+1)}}\right]$, were calculated for different grid sizes. The selected grid size consisted of 576153 domain elements, 65241 boundary elements, and 4884 edge elements, which was observed to be fair enough with a relative error of 1.16E-03 for the temperature difference and of 1.41E-02 for the pressure drop. Also, an iterative solution was used to solve the governing equations and a criterion of error ≤ 1E-06 was assumed small enough the convergence purpose. The temperature and flow rate were assumed to be uniform at the inlet of the channel, while a uniform pressure was assumed at the outlet. Constant heat flux boundary condition was applied at the lower surface of the cooling plate, and the inlet temperature of the coolant (water) is considered, while thermally isolated boundary condition was applied at the upper surface. Heat was assumed to be transferring from the side-edges of the plate to the surrounding through convection and radiation.

2.3.3. Data acquisition

The efficiency of fuel cell stacks increases at higher temperatures due to higher reaction rates on the reaction sites. The aim of this study is to investigate the hydrothermal performance of alumina nanofluids in cooling a PEM fuel cell depending on maximizing the efficiency of the entire plate by increasing the uniform temperature and controlling the maximum temperature. To achieve this aim, an index of uniform temperature (IUT) is presented through the entire volume of the cooling plate. IUT is a determining parameter which indicates the fuel cell's thermal performance. The lower is IUT, the more uniform temperature distribution is achieved [6]. IUT is calculated as follows [6]:

$$\mathrm{IUT} = \frac{\int_v |\mathrm{T}-\overline{\mathrm{T}}|\mathrm{dV}}{\int_v \mathrm{dV}}, \qquad (7)$$

$$where \quad \overline{\mathrm{T}} = \frac{\int_v \mathrm{T dV}}{\int_v \mathrm{dV}} \quad (8)$$

where $\overline{\mathrm{T}}$ is the volumetric mean temperature of the cooling plate.
The Reynolds number is calculated by [12]:

$$\mathrm{Re} = \frac{\rho_f u \mathrm{D_h}}{\mu_f} \quad (9)$$

where ρ_f is the density of either the base fluid or the nanofluid [kg/m^3], u is the uniform inlet velocity of the cooling fluid [m/s], D_h is the hydraulic diameter of the cooling channel [m], which is calculated as follows [12]:

$$\mathrm{D_h} = \frac{2\mathrm{WW}}{\mathrm{W+W}} = \mathrm{W} \quad (10)$$

where W is the cross-section's side length of the cooling channel, [m]. Finally, the pumping power can be expressed by the following equation [12]:

$$\mathrm{Pp} = u \,.\, \Delta\mathrm{p} \,.\, \mathrm{A_{cs}} \quad (11)$$

where Pp is the pumping power [W] and $\mathrm{A_{cs}}$ is the cross-section area of the channel [m^2].

3. Results and discussion

For validation purposes, four flow rates were adopted, namely: 20, 30, 40, and 50 ml/min. The experimental temperature differences between the outlet and inlet of the cooling plate (ΔT) were compared with those obtained from the CFD model. The results in Figure 7 shows that very good agreement was achieved between the experimental and modelling data, with percentage error less than 1.5. It is obvious that the CFD results are within the accuracy of the thermocouples (i.e., 0.3 ^{o}C). This agreement supports the assumptions that were used in solving the governing equations.

As mentioned earlier, the uniformity of temperature within the cooling plate, and consequently within the delegate layers, is crucially important for the durability of PEM

fuel cells. The IUT is an indicator for the uniformity of the temperature: the lower is the IUT , the better is the uniformity of temperature [45]. The IUT was calculated according to the Eqn. (7) and the results are shown in Figure 8. It is clear that the IUT decreases as the V_f increases, which ensures better temperature uniformity, lower thermal stresses and ultimately better longevity for the fuel cell. However, this requires higher pumping power. Also, it is obvious that adding nanoparticles to the base fluid has a negative effect on the IUT, and this effect is more obvious with lower flow rates. This could be attributed to the fact that when the nanoparticles concentration increases, the C_p of the coolant decreases and consequently the ΔT increases (see Figure 4 and Figure 7).

Eqn. (3) shows direct relationship between the pressure gradient and both velocity and viscosity of the nanofluids. Hence, it is expected that the pressure drop (Δp) across the cooling plate increases as the volume flow rate (in other word, velocity) of the coolant increases, and as the nanoparticles concentration increases due to the increase in the effective viscosity of the coolant. Figure 9 shows the results of Δp obtained from the CFD model. Figure 9 (a) shows a linear relationship between the (Δp) and Ø, and the slope (m) of the trendlines increases as V_f increases. This linear relationship is expected since the relationship between the effective viscosity and Ø is linear (see Figure 4). Figure 9(b) shows a nonlinear (exponential) relationship between (Δp) and V_f, and this is because (Δp) is directly proportional to the square power of the flow velocity, according to Darcy-Weisbach equation. Also, it is obvious that, contrary to the IUT, (Δp) becomes more sensitive to Ø when V_f becomes higher; implying extra pumping costs.

The calculated pumping power (Pp) can be seen in Figure 10 as function of the V_f and Ø. As expected, the Pp increases as V_f increases, and it becomes more sensitive to Ø with increasing Pp.

To examine the effectiveness (ε) of using nanofluids as a cooling fluid and the required pumping power (pumping cost, Pc), the IUT data were differentiated with respect to Pp and the Pp data were differentiated with respect to the IUT. In other words, ε is the rate of change of IUT with Pp, while Pc is the rate of change of Pp with IUT. The results can be seen in Figure 11. It is clear that the sensitivity of ε to Ø decreases as V_f increases. Also, the ε of using water is higher than using nanofluids especially at the low flow rates. In other words, water is more effective than nanofluids in terms of dissipating heat, where the maximum percentage of the effectiveness reduction of the nanofluids, which was calculated as $\frac{\varepsilon_{H2O}-\varepsilon_{nf}}{\varepsilon_{H2O}} * 100$, is 7.9% at $V_f = 20$ ml/min. Furthermore, the Pc (the pumping power required to reduce the IUT by 1 ºC) for water is lower than Pc for nanofluids, and the sensitivity of Pc to Ø becomes higher at higher V_f, where the maximum percentage of the pumping cost, which was calculated as $\frac{Pc_{nf}-Pc_{H2O}}{Pc_{H2O}} * 100$, is 6% at $V_f = 50$ ml/min.

As mentioned earlier, most relevant investigations in the literature present the thermal performance of the nanofluids as a function of Reynolds number (Re). Therefore, it is of interest to present our results as a function of Re. To achieve this, the relationship between Re and V_f must be investigated. The data of Re were calculated using Eqn. (9) and the results are shown in Figure 12. Linear relationships between Re and V_f are obtained. It is clear that, for a given V_f, Re decreases as Ø increases. This is because the effective viscosity increases as nanoparticles concentration increases. The figure also shows that the slope of the trendlines decreases as Ø increases. This is attributed to the thermophysical properties of the nanofluids (Figure 4). This result supports our claim, which states that the enhancement in the thermal performance of nanofluids presented in most of the published papers is due to the extra flow rate required to maintain Re constant.

Figure 13 shows IUT as a function of Re and Ø. It is clear that the thermal performance improves when using nanofluids. Namely, for a given Re, IUT decreases as Ø increases. However, this result is misleading, and that is why we have suggested to use the pumping power as an independent variable to investigate the thermal performance of using nanofluids.

Figure 14 shows IUT as a function of Pp and Ø. It is obvious that, the IUT decreases as the Pp increases, and increases as Ø increases. In other words, for a given pumping power, the performance of water is better than nanofluids, as the lower IUT insures better temperature distribution and lower difference between the maximum and the mean temperatures. This means using water leads to efficient performance and longer lifespan of the PEM fuel cells [4,5].

4. Conclusions

Due to their superior thermal conductivity, recent studies have proposed nanofluids as alternative heat transfer fluids for PEM fuel cells. However, although the thermophysical properties of a nanofluid depend on its concentration, Reynolds number was used as an independent variable in those parametric studies. As Reynolds number is a function of the density, velocity, and viscosity of a fluid, it seems that adopting Reynolds number as an independent parameter is misleading. In this study, a well-validated, comprehensive, 3-D CFD model has been built to investigate the impact of using alumina nanofluids as a coolant for PEM fuel cells on the hydrothermal performance and the pumping power. Different concentrations of the nanofluid were prepared and characterized. The density, specific heat capacity, thermal conductivity and viscosity were measured and subsequently fed into the CFD model. The main results show that:

- The index of uniform temperature (IUT) as a function of Reynolds number decreases when the concentration of the nanofluid increases, presenting better thermal performance.

- The index of uniform temperature (IUT) as a function of flow rate and pumping power increases when the concentration of the nanofluid increases, presenting worse thermal performance.

Two main conclusions could be drawn from this study, one general and one specific. The general conclusion is that it is not correct to use Reynolds number (or any other dimensionless number such as Nusselt number) as an independent (or dependent) variable in analysing the hydrothermal performance of nanofluids because of the dependency of these parameters on all or some of the thermophysical properties of the nanofluids which are all functions of the concentration. Adopting such an approach leads to false conclusions. While the specific conclusion is that aqueous alumina nanofluids cannot offer feasible benefits in terms of cooling PEM fuel cells as water is more effective.

References

[1] Barbir F. Fuel Cell Basic Chemistry and Thermodynamics, in: PEM Fuel Cells, 2nd ed., Elsevier, 2013: pp. 17–32. https://doi.org/10.1016/B978-0-12-387710-9.00002-3.

[2] Pichonat T. MEMS-Based Micro Fuel Cells as Promising Power Sources for Portable Electronics, in: T.S. Zhao (Ed.), Micro Fuel Cells, Elsevier, 2009: pp. 51–97. https://doi.org/10.1016/B978-0-12-374713-6.00002-0.

[3] Singh R, Oberoi AS, Singh T. Factors influencing the performance of PEM fuel cells: A review on performance parameters, water management, and cooling techniques. Int J Energy Res 2022; 46:3810–3842. https://doi.org/10.1002/er.7437.

[4] Yu Y, Chen M, Zaman S, Xing S, Wang M, Wang H. Thermal management system for liquid-cooling PEMFC stack: From primary configuration to system control strategy. eTransportation 2022;12, 100165. https://doi.org/10.1016/j.etran.2022.100165.

[5] Lochner T, Kluge RM, Fichtner J, ElSayed HA, Garlyyev B, Bandarenka A.S. Temperature Effects in Polymer Electrolyte Membrane Fuel Cells. ChemElectroChem 2020; 7:3545–3568. https://doi.org/10.1002/celc.202000588.

[6] Chen FC, Gao Z, Loutfy RO, Hecht M. Analysis of Optimal Heat Transfer in a PEM Fuel Cell Cooling Plate. Fuel Cells 2003; 3:181–188. https://doi.org/10.1002/fuce.200330112.

[7] Rahgoshay SM, Ranjbar AA, Ramiar A, Alizadeh E. Thermal investigation of a PEM fuel cell with cooling flow field. Energy 2017; 134:61–73. https://doi.org/10.1016/j.energy.2017.05.151.

[8] Afshari E, Ziaei-Rad M, Dehkordi MM. Numerical investigation on a novel zigzag-shaped flow channel design for cooling plates of PEM fuel cells. J Energy Inst 2017; 90:752–763. https://doi.org/10.1016/j.joei.2016.07.002.

[9] Alizadeh E, Rahgoshay SM, Rahimi-Esbo M, Khorshidian M, Saadat SHM. A novel cooling flow field design for polymer electrolyte membrane fuel cell stack. Int J Hydrogen Energy 2016; 41:8525–8532. https://doi.org/10.1016/j.ijhydene.2016.03.187.

[10] Saeedan M, Afshari E, Ziaei-Rad M. Modeling and optimization of turbulent flow through PEM fuel cell cooling channels filled with metal foam- a comparison of water and air cooling systems. Energy Convers Manag 2022; 258,115486. https://doi.org/10.1016/j.enconman.2022.115486.

[11] Afshari E, Ziaei-Rad M, Shariati Z. A study on using metal foam as coolant fluid distributor in the polymer electrolyte membrane fuel cell. Int J Hydrogen Energy 2016; 41:1902–1912. https://doi.org/10.1016/j.ijhydene.2015.10.122.

[12] Arear WF, Zeiny A, Al-Baghdadi M. Influence of Al 2 O3-Water Nanofluid Coolant on Thermal Performance of Hydrogen PEM Fuel Cell Stacks. IOP Conf Ser Mater Sci Eng 2021; 1094, 012064. https://doi.org/10.1088/1757-899X/1094/1/012064.

[13] Spiegel C. Mathematical Modeling of Polymer Exchange Membrane Fuel Cells. University of South Florida, 2008. Available online:"Mathematical Modeling of Polymer Exchange Membrane Fuel Cells" by Colleen Spiegel (usf.edu).

[14] Shabani B, Andrews J. An experimental investigation of a PEM fuel cell to supply both heat and power in a solar-hydrogen RAPS system. Int J Hydrogen Energy 2011; 36:5442–5452. https://doi.org/10.1016/j.ijhydene.2011.02.003.

[15] Choi SUS, Eastman JA. Enhancing thermal conductivity of fluids with nanoparticles. Proceeding ASME Int Mech Eng Congr Expo 1995;66. Available online: (13) (PDF) Enhancing thermal conductivity of fluids with nanoparticles (researchgate.net).

[16] Shi Y, Abidi A, Khetib Y, Zhang L, Sharifpur M, Cheraghian G. The computational study of nanoparticles shape effects on thermal behavior of H2O-Fe nanofluid: A molecular dynamics approach. J Mol Liq 2022;346,117093. https://doi.org/10.1016/j.molliq.2021.117093.

[17] Younes H, Mao M, Sohel Murshed SM, Lou D, Hong H, Peterson GP. Nanofluids: Key parameters to enhance thermal conductivity and its applications. Appl Therm Eng 2022; 207, 118202. https://doi.org/10.1016/j.applthermaleng.2022.118202.

[18] Li X, Yuan F, Tian W, Dai C, Yang X, Wang D, Du J, Yu W, Yuan H. Heat Transfer Enhancement of Nanofluids with Non-Spherical Nanoparticles: A Review. Appl Sci 2022; 12, 4767. https://doi.org/10.3390/app12094767.

[19] Almurtaji S, Ali N, Teixeira JA, Addali A. On the Role of Nanofluids in Thermal-hydraulic Performance of Heat Exchangers—A Review. Nanomaterials 2020; 10, 734. https://doi.org/10.3390/nano10040734.

[20] Bakthavatchalam B, Habib K, Saidur R, Saha BB, Irshad K. Comprehensive study on nanofluid and ionanofluid for heat transfer enhancement: A review on current and future perspective. J Mol Liq 2020; 305, 112787. https://doi.org/10.1016/j.molliq.2020.112787.

[21] Buongiorno J. Convective Transport in Nanofluids. J Heat Transfer 2006; 128:240–250. https://doi.org/10.1115/1.2150834.

[22] Bargal MHS, Abdelkareem MAA, Tao Q, Li J, Shi J, Wang Y. Liquid cooling techniques in proton exchange membrane fuel cell stacks: A detailed survey. Alexandria Eng J 2020; 59:635–655. https://doi.org/10.1016/j.aej.2020.02.005.

[23] Khani M, Habibzadeh S, Moraveji MK, Ebrahim HA, Alizadeh J. Novel α-alumina@CuO-Fe2O3nanofluid for potential application in PEM fuel cell cooling systems: Towards neutralizing the increase of electrical conductivity. Thermochim Acta 2021; 695, 178818. https://doi.org/10.1016/j.tca.2020.178818.

[24] Khalid S, Zakaria I, Azmi WH, Mohamed WANW. Thermal–electrical–hydraulic properties of Al2O3–SiO2 hybrid nanofluids for advanced PEM fuel cell thermal management. J Therm Anal Calorim 2021; 143:1555–1567. https://doi.org/10.1007/s10973-020-09695-8.

[25] Johari MNI, Zakaria IA, Azmi WH, Mohamed WANW. Green bio glycol Al2O3-SiO2 hybrid nanofluids for PEMFC: The thermal-electrical-hydraulic perspectives. Int Commun Heat Mass Transf 2022; 131, 105870. https://doi.org/10.1016/j.icheatmasstransfer.2021.105870.

[26] Zakaria I, Azmi WH, Mohamed WANW, Mamat R, Najafi G. Experimental Investigation of Thermal Conductivity and Electrical Conductivity of Al2O3 Nanofluid in Water - Ethylene Glycol Mixture for Proton Exchange Membrane Fuel Cell Application. Int Commun Heat Mass Transf 2015; 61:61–68. https://doi.org/10.1016/j.icheatmasstransfer.2014.12.015.

[27] Shen LP, Wang H, Dong M, Ma ZC, Wang HB. Solvothermal synthesis and electrical conductivity model for the zinc oxide-insulated oil nanofluid. Phys Lett A 2012; 376:1053–1057. https://doi.org/10.1016/j.physleta.2012.02.006.

[28] Kumar N, Sonawane SS, Sonawane SH. Experimental study of thermal conductivity, heat transfer and friction factor of Al2O3 based nanofluid. Int Commun Heat Mass Transf 2018; 90: 1–10. https://doi.org/10.1016/j.icheatmasstransfer.2017.10.001.

[29] Li H, Wang L, He Y, Hu Y, Zhu J, Jiang B. Experimental investigation of thermal conductivity and viscosity of ethylene glycol based ZnO nanofluids. Appl Therm Eng 2015; 88: 363–368. https://doi.org/10.1016/j.applthermaleng.2014.10.071.

[30] Khdher AM, Sidik NAC, Hamzah WAW, Mamat R. An experimental determination of thermal conductivity and electrical conductivity of bio glycol based Al2O3 nanofluids and development of new correlation. Int Commun Heat Mass Transf 2016; 73:75–83. https://doi.org/10.1016/j.icheatmasstransfer.2016.02.006.

[31] Usri NA, Azmi WH, Mamat R, Hamid KA, Najafi G. Thermal Conductivity Enhancement of Al2O3 Nanofluid in Ethylene Glycol and Water Mixture. Energy Procedia 2015; 79:397–402. https://doi.org/10.1016/j.egypro.2015.11.509.

[32] Bargal MHS, Souby MM, Abdelkareem MAA, Sayed M, Tao Q, Chen M,

Wang Y. Experimental investigation of the thermal performance of a radiator using various nanofluids for automotive PEMFC applications. Int J Energy Res 2021; 45:6831– 6849. https://doi.org/10.1002/er.6274

[33] Tao Q, Su C, Chen M, Deng Y, Wang Y, Li J, Bargal MHS. Experimental investigation on heat transfer enhancement of a radiator in a simulated pemfc cooling system using hexagonal boron nitride nanofluids. Heat Transf Res 2021; 52:31–45. https://doi.org/10.1615/HeatTransRes.2021036147 .

[34] Tao Q, Su C, Chen M, Deng Y, Wang Y, Yu M, Sun H, Bargal MHS. Numerical investigation on the temperature distribution inside the engine compartment of a fuel cell vehicle with nanofluids as coolant. Int J Energy Res 2021; 45:9613–9626. https://doi.org/10.1002/er.6485.

[35] Zakaria I, Mohamed WANW, Mamat AMIB, Saidur R, Azmi WH, Mamat R, Talib SFA. Experimental Investigation of Al2O3 - Water Ethylene Glycol Mixture Nanofluid Thermal Behaviour in a Single Cooling Plate for PEM Fuel Cell Application. Energy Procedia 2015; 79:252–258. https://doi.org/10.1016/j.egypro.2015.11.474.

[36] Zakaria IA, Mohamed WANW, Zailan MB, Azmi WH. Experimental analysis of SiO2-Distilled water nanofluids in a Polymer Electrolyte Membrane fuel cell parallel channel cooling plate. Int J Hydrogen Energy 2019; 44:25850–25862. https://doi.org/10.1016/j.ijhydene.2019.07.255.

[37] Usri NA, Azmi WH, Mamat R, Hamid KA, Najafi G. Heat Transfer Augmentation of Al2O3 Nanofluid in 60:40 Water to Ethylene Glycol Mixture. Energy Procedia 2015; 79: 403–408. https://doi.org/10.1016/j.egypro.2015.11.510.

[38] Guzei DV, Minakov AV, Rudyak VY. On efficiency of convective heat transfer of nanofluids in laminar flow regime. Int J Heat Mass Transf 2019; 139: 180–192. https://doi.org/10.1016/j.ijheatmasstransfer.2019.05.016.

[39] Khetib Y, Alzaed A, Tahmasebi A, Sharifpur M, Cheraghian G. Influence of using innovative turbulators on the exergy and energy efficacy of flat plate solar collector with DWCNTs-TiO2/water nanofluid. Sustain Energy Technol Assessments 2022; 51, 101855. https://doi.org/10.1016/j.seta.2021.101855.

[40] Nadim Zarizi, Zakaria IA, Johari MNI, Wan Mohamed WAN, Raja Ahsan Shah RM. Thermo-Electrical Behavior of Al2O3 and SiO2 Nanofluids in A Proton-Exchange Membrane Fuel Cell (PEMFC) Cooling Channel. Pertanika J Sci Technol 2022; 30:1381–1396. https://doi.org/10.47836/pjst.30.2.29.

[41] Muhammad Syafiq Idris, Irnie Azlin Zakaria, Wan Azmi Wan Hamzah, Wan Ahmad Najmi Wan Mohamed. The Characteristics of Hybrid Al2O3:SiO2 Nanofluids in Cooling Plate of PEMFC. J Adv Res Fluid Mech Therm Sci 2021;88:96–109. https://doi.org/10.37934/arfmts.88.3.96109.

[42] Mohamad Noor Izwan Johari, Irnie Azlin Zakaria, Nur Syahirah Mohammed Affendy. Thermal Behaviour of Hybrid Nanofluids in Water: Bio Glycol Mixture in Cooling Plates of PEMFC. CFD Lett 2022; 14: 43–55. https://doi.org/10.37934/cfdl.14.6.4355.

[43] Zakaria IA, Mohamed WANW, Azid NHA, Suhaimi MA, Azmi WH. Heat transfer and electrical discharge of hybrid nanofluid coolants in a fuel cell cooling channel application. Appl Therm Eng 2022; 210, 118369. https://doi.org/10.1016/j.applthermaleng.2022.118369.

[44] Retamal Marín RR, Babick F, Stintz M. Ultrasonic dispersion of nanostructured materials with probe sonication − practical aspects of sample preparation. Powder Techno 2017; 318: 451–458. https://doi.org/10.1016/j.powtec.2017.05.049.

[45] Zhai Y, Li L, Wang J, Li Z. Evaluation of surfactant on stability and thermal performance of Al2O3-ethylene glycol (EG) nanofluids. Powder Techno. 2019; 343: 215–224. https://doi.org/10.1016/j.powtec.2018.11.051.

[46] Zakaria I, Mohamed WANW, Azmi WH, Mamat AMI, Mamat R, Daud WRW. Thermo-electrical performance of PEM fuel cell using Al2O3 nanofluids. Int J Heat Mass Transf 2018; 119: 460–471. https://doi.org/10.1016/j.ijheatmasstransfer.2017.11.137.

[47] Zeiny A., Jin H, Bai L, Lin G, Wen D. A comparative study of direct absorption nanofluids for solar thermal applications. Sol Energy 2018; 161:74–82. https://doi.org/10.1016/j.solener.2017.12.037.

[48] Tian MW, Khetib Y, Yan SR, Rawa M, Sharifpur M, Cheraghian G, Melaibari A.A. Energy, exergy and economics study of a solar/thermal panel cooled by nanofluid. Case Stud Therm Eng 2021; 28, 101481. https://doi.org/10.1016/j.csite.2021.101481.

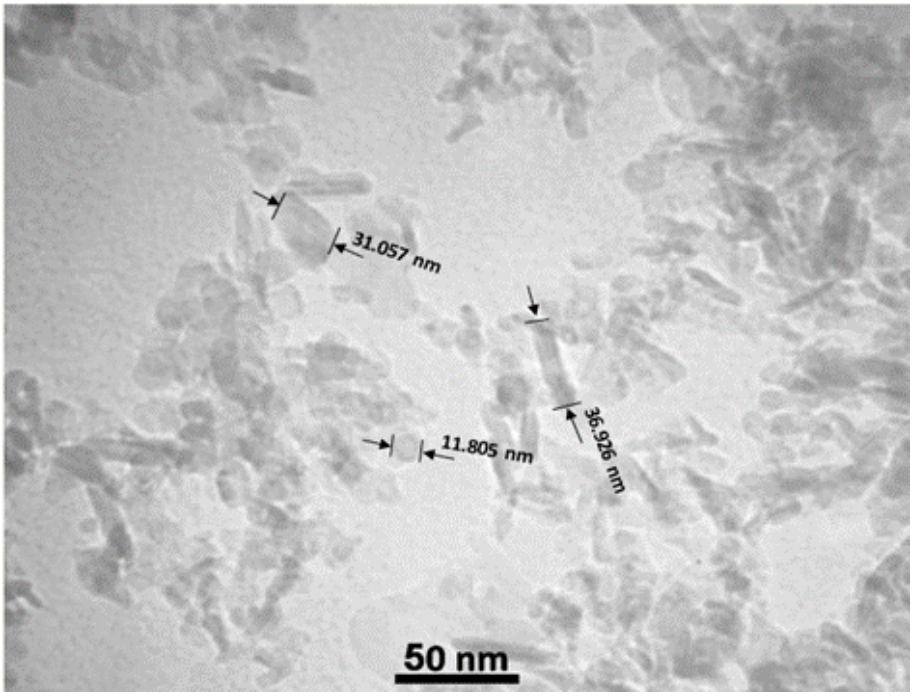

Figure 1 TEM picture of the prepared Al_2O_3 aqueous nanofluid.

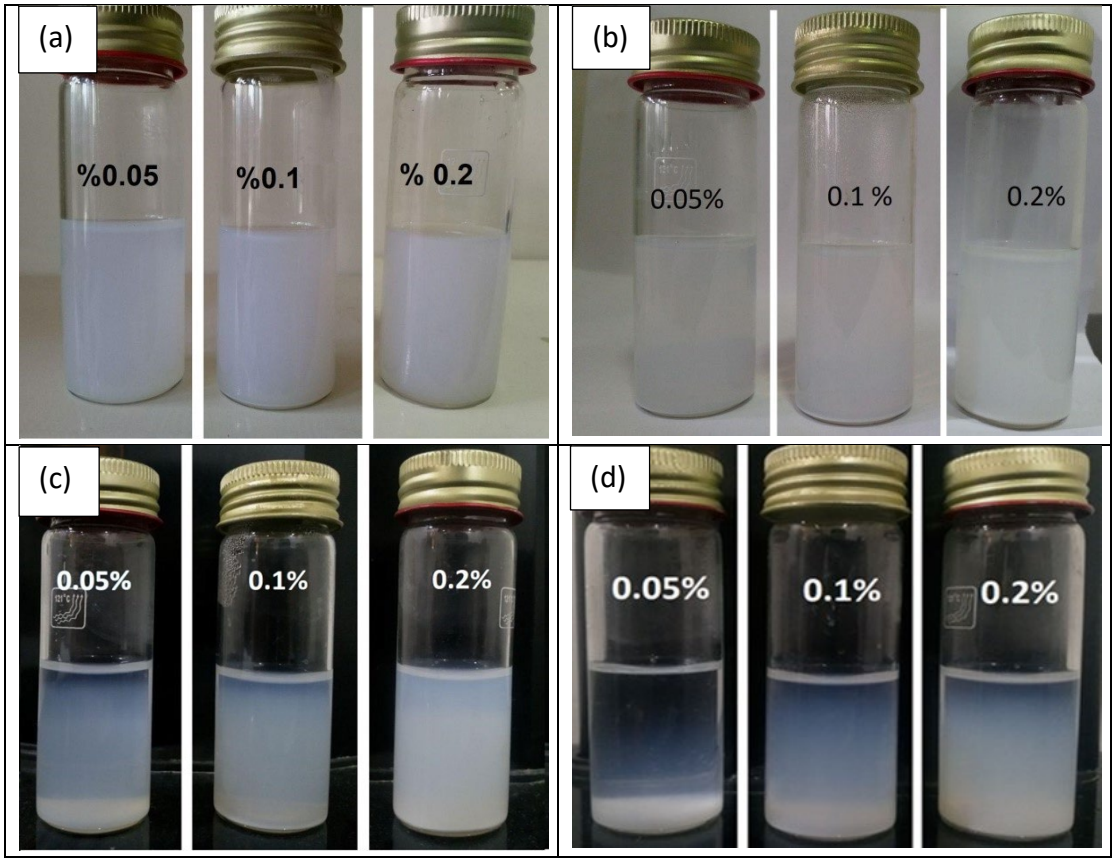

Figure 2 photographic pictures of the prepared Al_2O_3 aqueous nanofluids after: (a) one day, (b) two days, (c) 7 days, and (d) 30 days.

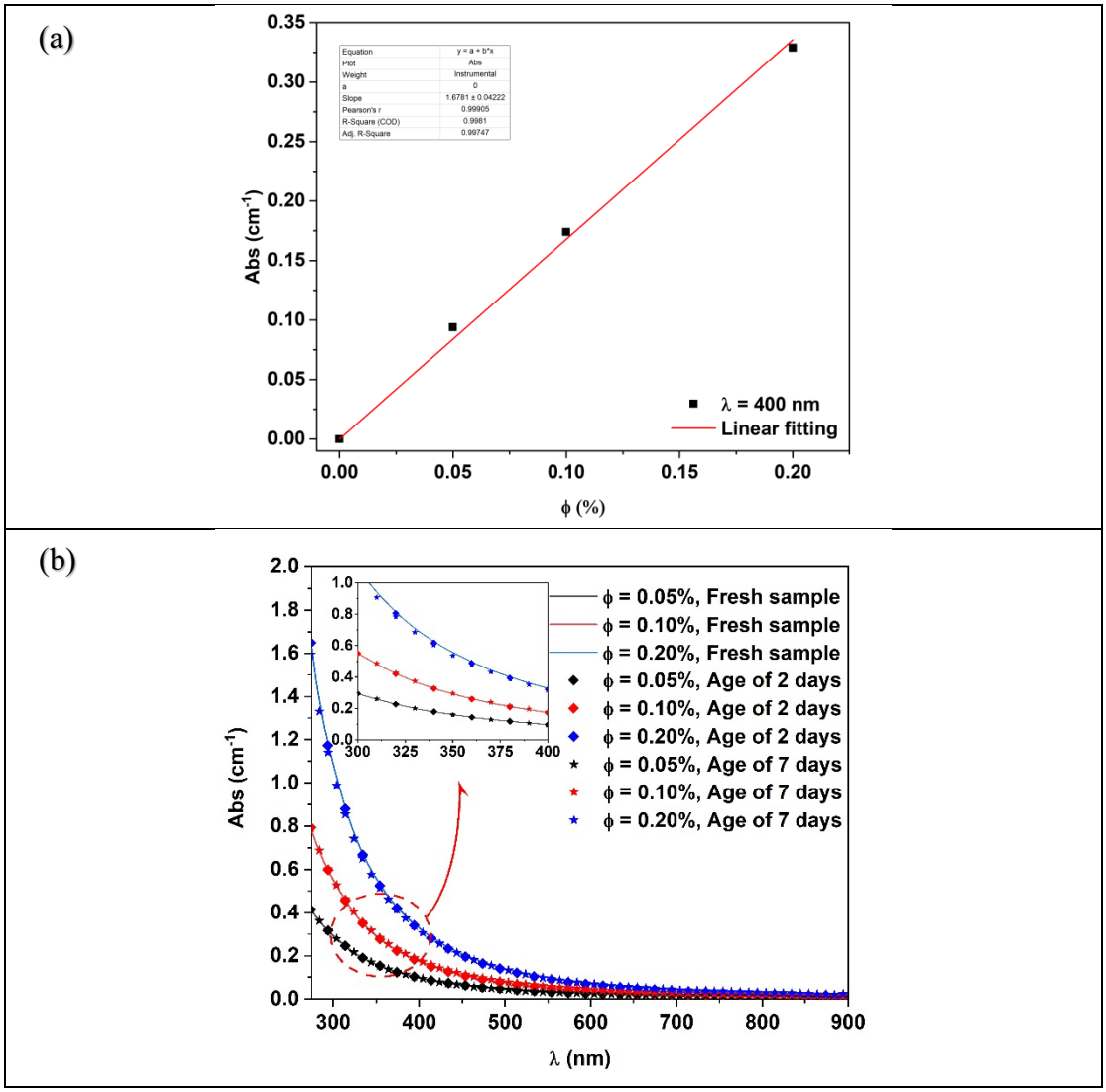

Figure 3 UV-Vis Spectrophotometry results. (a) the linear relationship between the absorbance of the nanofluid and its concentration, (b) the spectral absorbance the nanofluid as a function of its concentration and age.

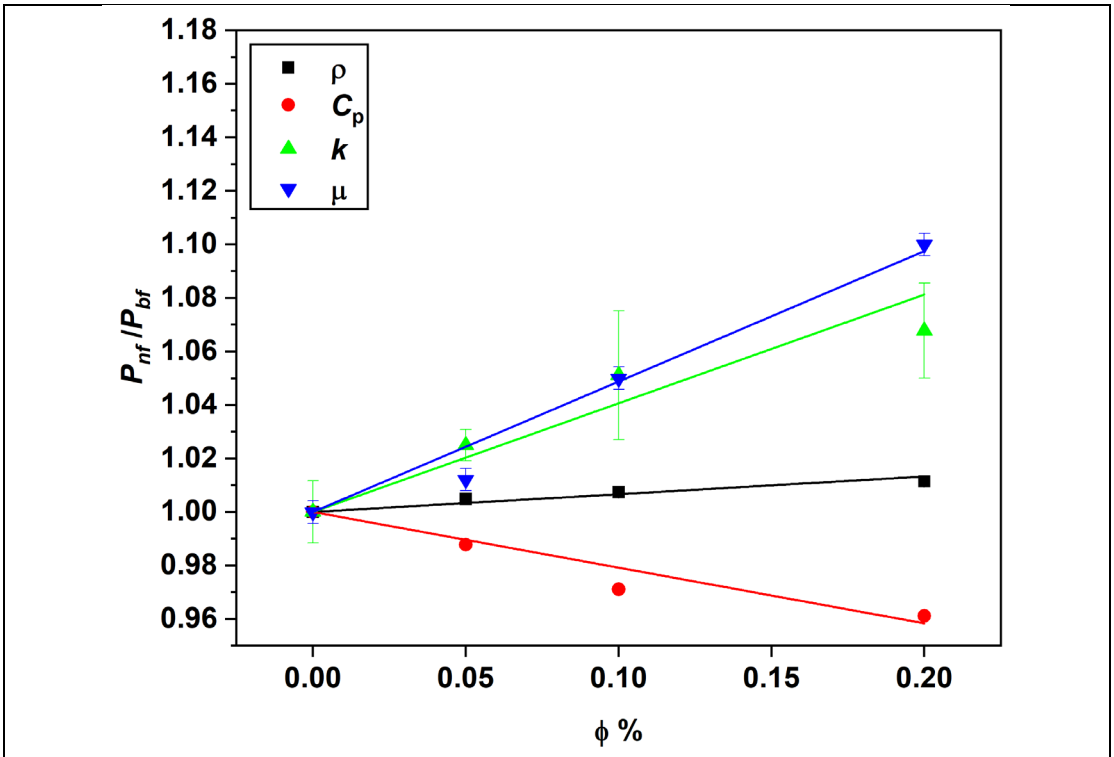

	Mean Value/Standard Deviation			
Ø%	ρ [kg/m^3]	C_p [J/kg.K]	k [W/m.K]	μ [Pa.s]
0	0.9689/3.6E-5	4180/6.9E-4	0.6/1.2E-2	0.7833/1.1E-2
0.05	0.9736/3.0E-4	4129/7.7E-4	0.615/5.9E-3	0.7895/4.2E-3
0.1	0.9761/6.6E-4	4059/6.1E-4	0.6307/2.4E-2	0.8163/4.5E-3
0.2	0.98/5.9E-4	4017/4.9E-4	0.6407/1.8E-2	0.8606/1.6E-3

Figure 4 Thermophysical properties of nanofluids and their standard deviation.

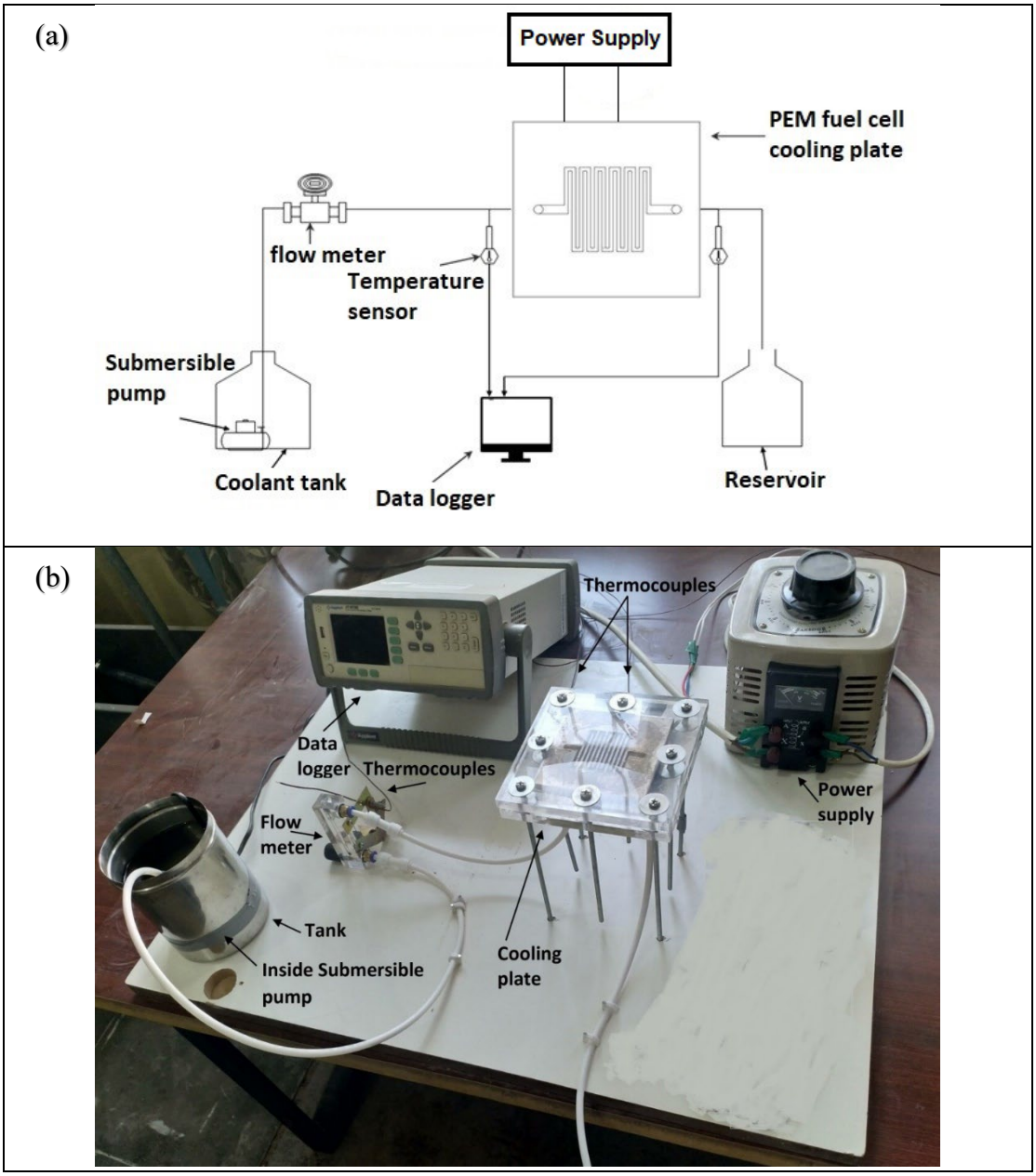

Figure 5 Experimental set-up: (a) schematic diagram and (b) photographic picture.

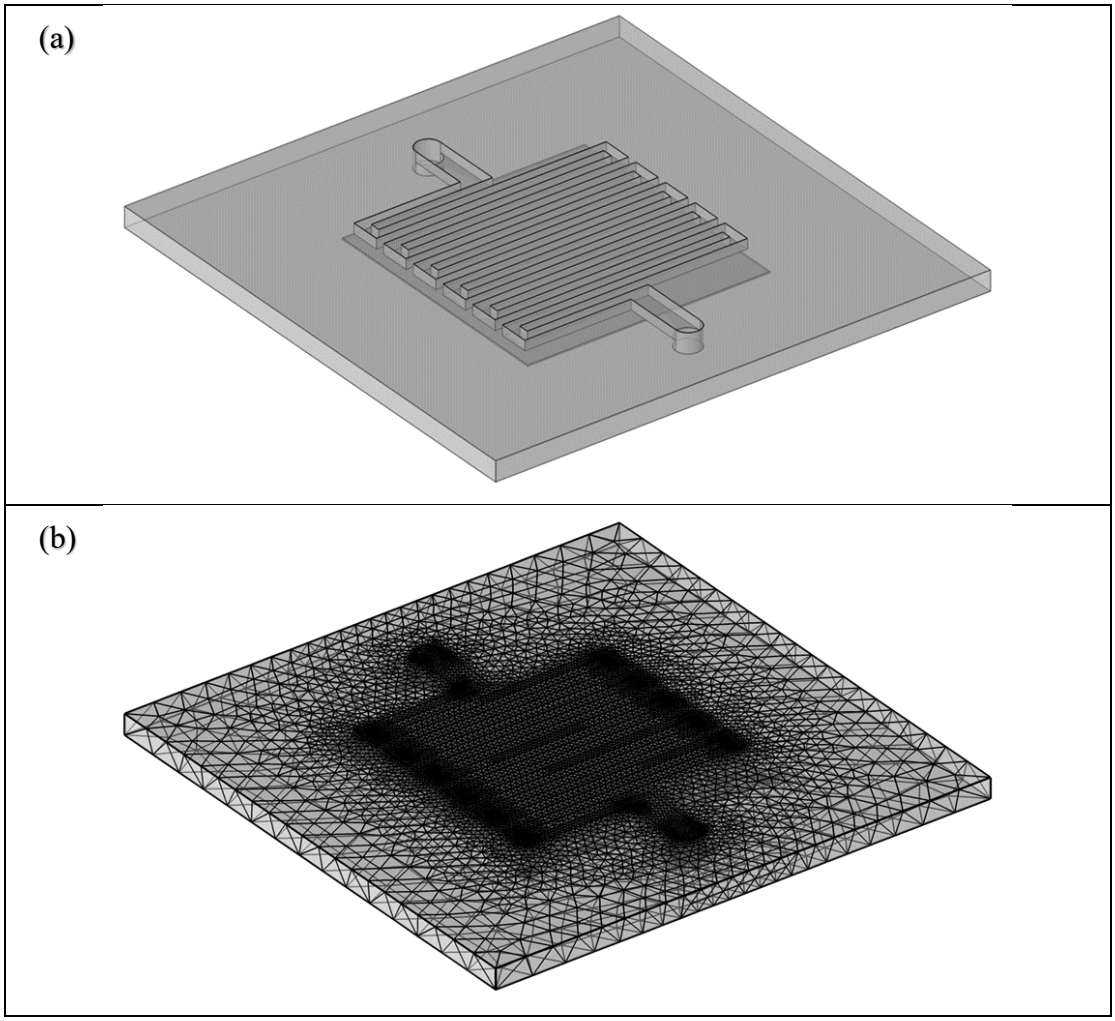

Figure 6 The computational domain (a) and mesh (b).

Table 1. The physical properties of the aluminum cooling plate.

Property	**Value**
Density [kg/m^3]	2730
Poisson's ratio	0.33
Expansion coefficient [K^{-1}]	$23.2*10^{-6}$
Thermal conductivity [W m^{-1} K^{-1}]	155
Heat capacity [J kg^{-1} K^{-1}]	893
Emissivity	0.6
Dimensions [mm]	100 x 100
Thickness [mm]	5

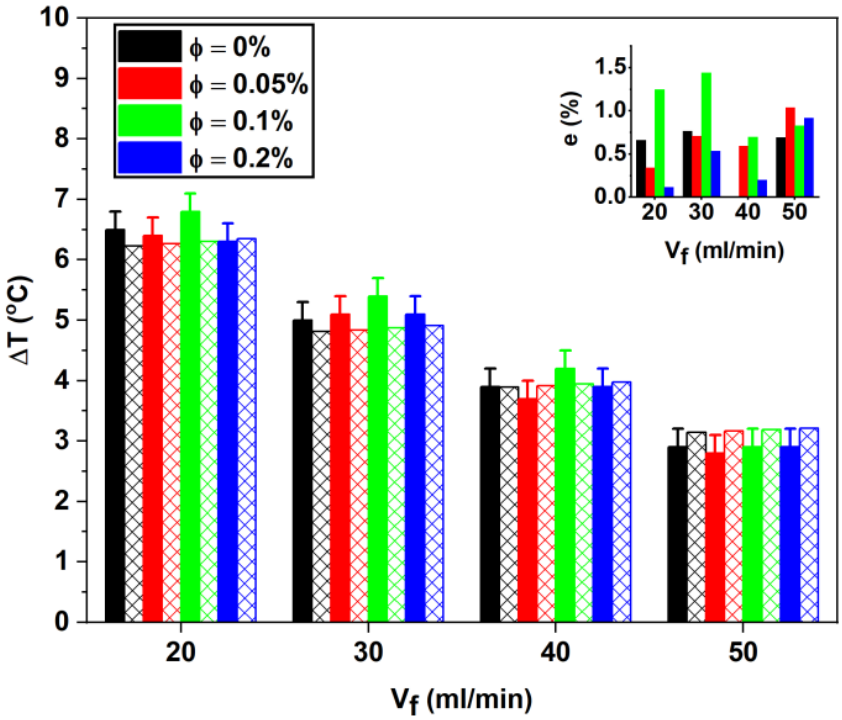

Figure 7 CFD model validation. Solid bars represent experimental results and patterned bars represent CFD results. Note that %e equals to $\frac{CFD-Exp}{Exp}100\%$.

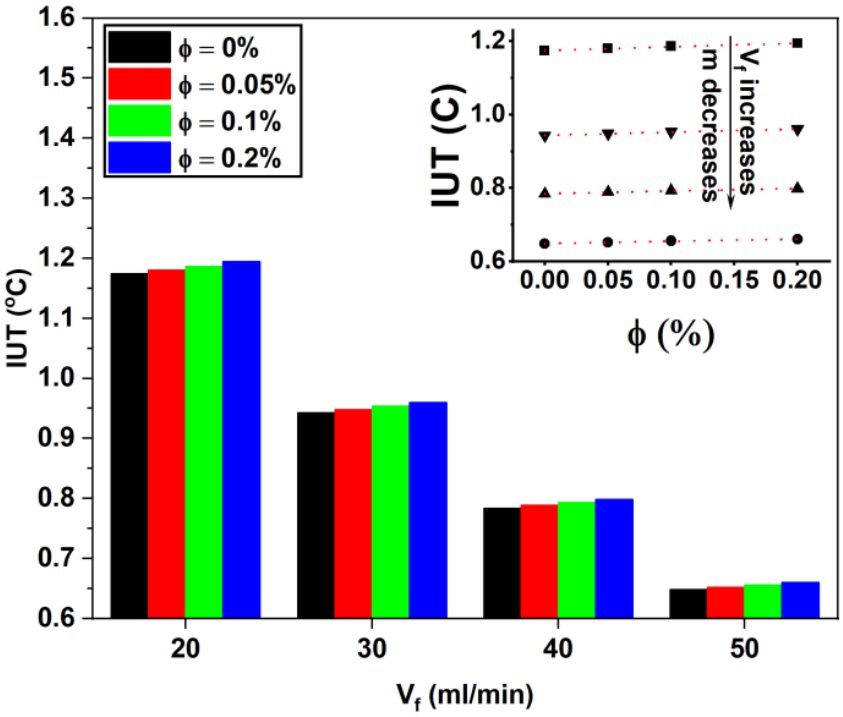

Figure 8 The index of uniform temperature (IUT) as a function of the flow rate of the coolant and as a function of the nanoparticles concentration (inset). Note that "m" is the slope of the trend lines (the dotted lines).

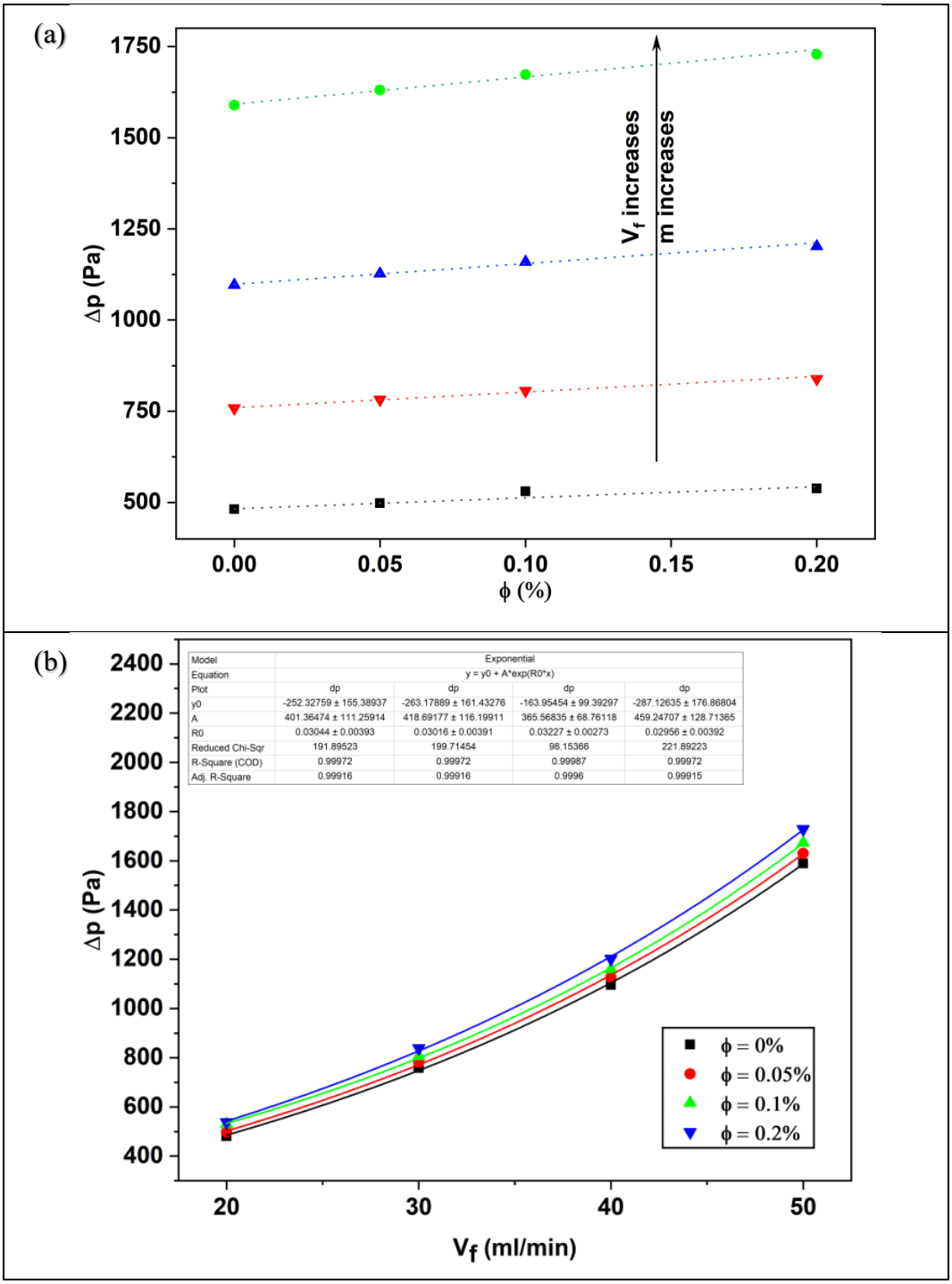

Figure 9 The pressure drop as a function of the volume flow rate and nanoparticles concentration in the form of: (a) bar and (b) scatter charts. Symbols represent the calculated values, and lines represent the trendlines.

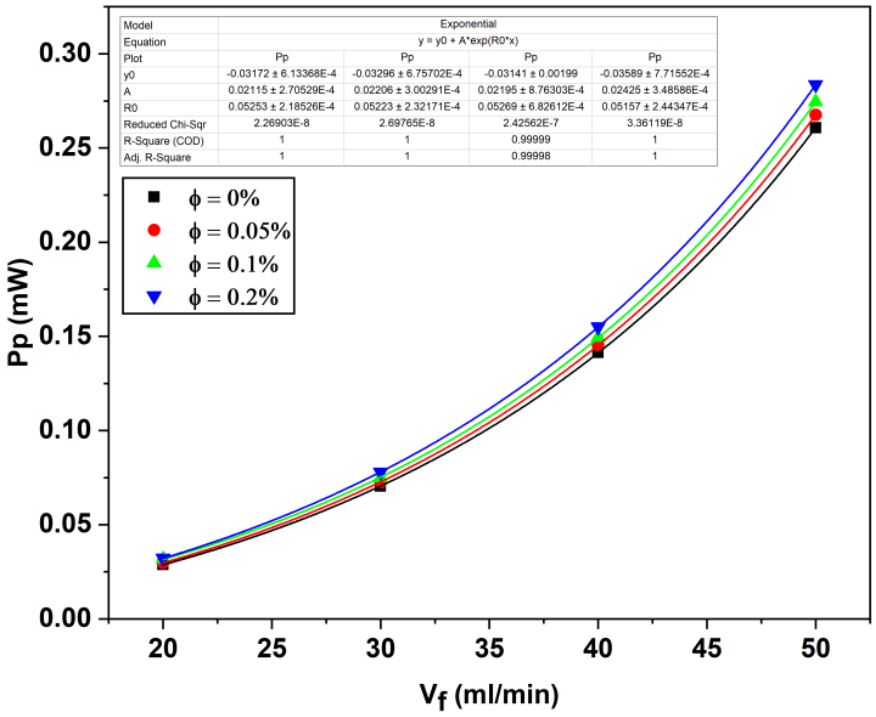

Figure 10 Pumping power as a function of coolant flowrate. Symbols represent calculated values, and lines represent trendlines.

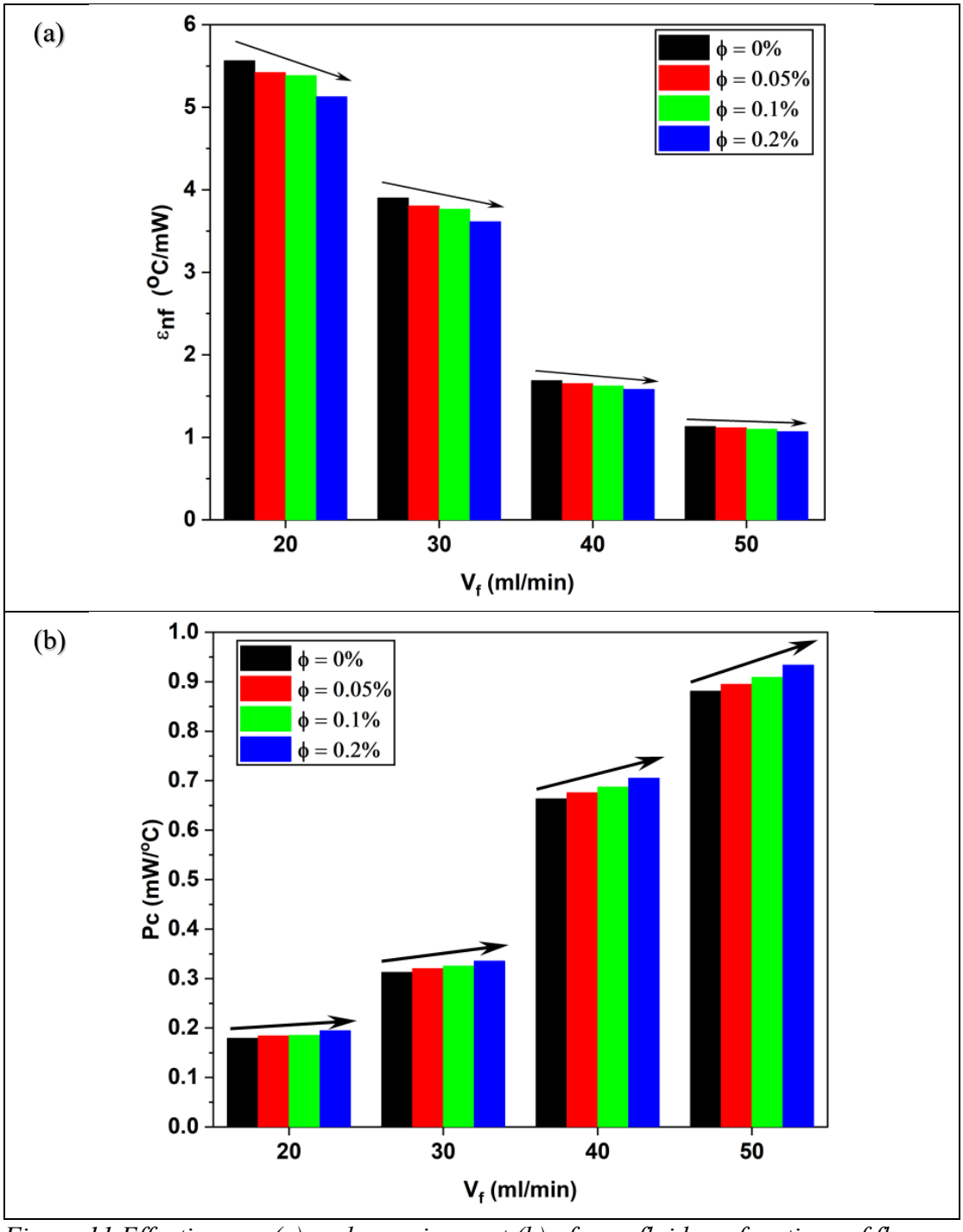

Figure 11 Effectiveness (a) and pumping cost (b) of nanofluids as functions of flow rate and nanoparticles concentration.

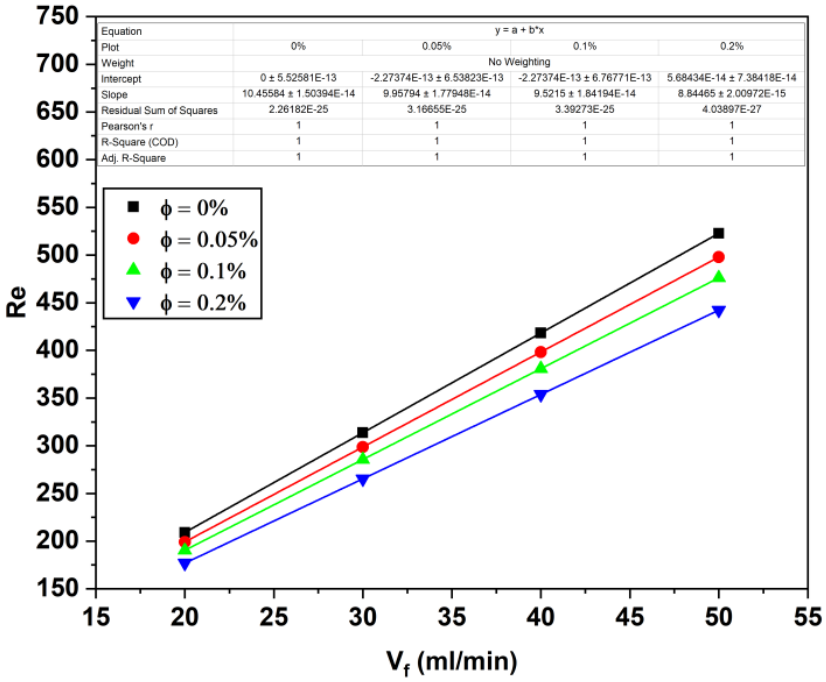

Figure 12 The Reynolds number (Re) as a function of flow rate and nanoparticles concentration. Symbols represent calculated values and lines represent trendlines.

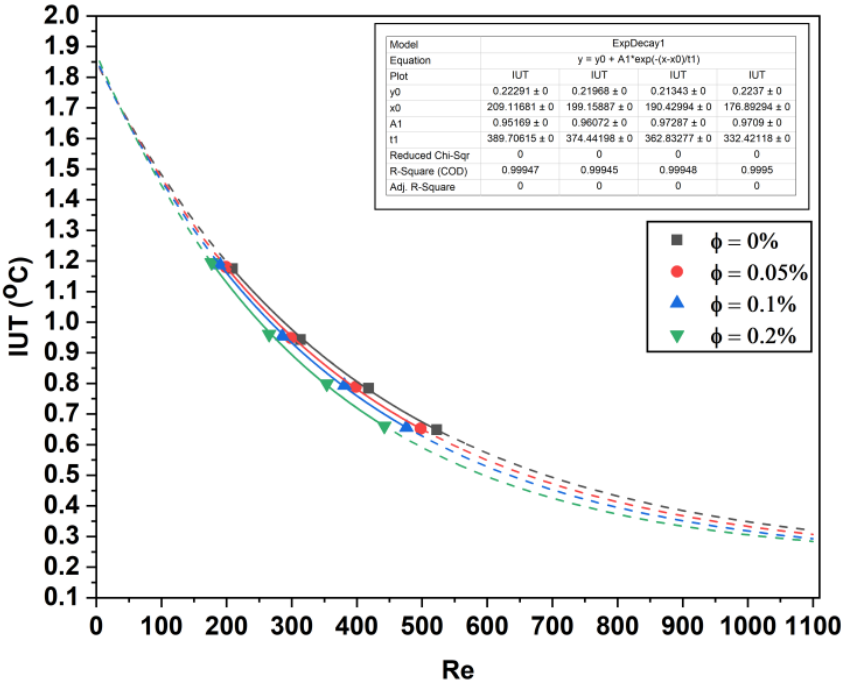

Figure 13 IUT as a function of Re and Ø. Symbols represent calculated values, solid lines represent trendlines, and dashed lines represent forecast values.

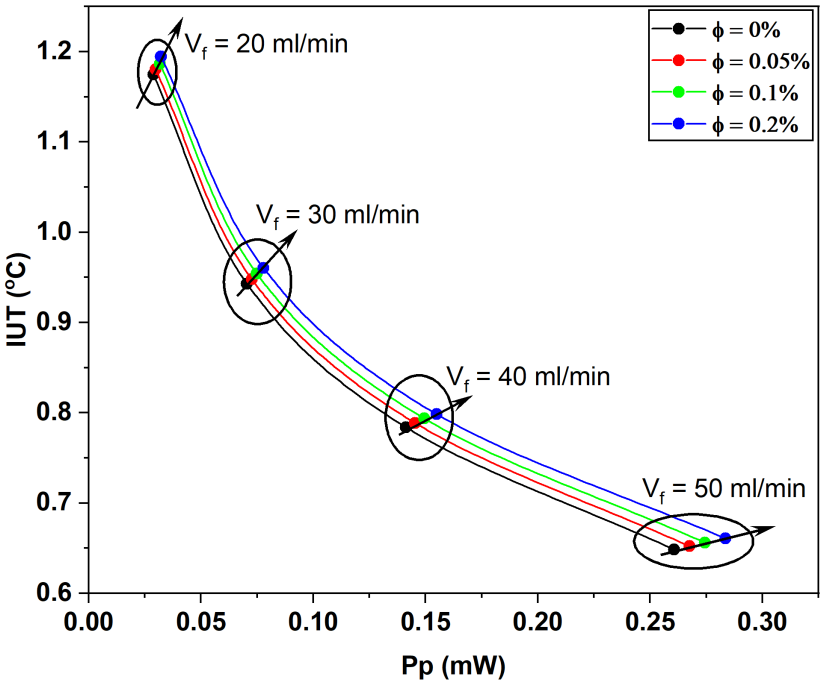

Figure 14 The index of uniform temperature(IUT) as a function of pumping power and concentration.